2.5 FRICTION STIR WELDING OF ODS STEELS AND ADVANCED FERRITIC STRUCTURAL STEELS — Z. Feng, Z. Yu, D. Hoelzer, M. A. Sokolov, and L. T. Tan (Oak Ridge National Laboratory)

OBJECTIVE

This project addresses the critical technology gap of joining oxide dispersion strengthened (ODS) steels, nanostructured ferritic alloys (NFAs), reduced-activation ferritic/martensitic (RAFM) steels, and dissimilar metal joining between ODS/NFAs and RAFM steels through friction stir welding technology. The research focuses on understanding the stability of the strengthening phases in the weld region, and the bonding mechanisms between dissimilar structural steels as a function of FSW process conditions.

Specific project objectives are (i) developing the process parameter space to consistently produce defect-free welds of the same and dissimilar metals, (ii) developing the knowledge base and practically applicable approaches to tailor and optimize the microstructure features in the weld to match the properties of the base metal through process innovation, and (iii) producing representative weld joints and welded components to support future testing and evaluation at high temperature and irradiation environments in collaboration with JAEA and other international collaborators.

SUMMARY

Initial friction stir trial welds were made on ODS alloy MA965, RAFM steels EUROFER97 and F82H, and between MA956 and EUROFER97 (dissimilar weld). Defect-free similar and dissimilar welds were obtained. The microstructure of the welded region was characterized using optical microscopy (OM) and small-angle neutron scattering (SANS). OM examination showed that the microstructures in the stir zone (SZ), thermo-mechanically affected zone (TMAZ) and heat affect zone (HAZ) were significantly different from these in the base metal (BM). Small angle neutron scattering measurements were performed in the base metal and welded region to characterize the changes in nano-scale oxide features. Aggregation of the fine nano-scale particles was observed in the SZ. Micro-hardness mapping on the cross section of welds clearly revealed the effects of FSW.

PROGRESS AND STATUS

Introduction

Future fusion reactors will require utilization of advanced structural materials that must safely sustain the extremely hostile environment involving intense heat fluxes, high temperatures, reactive chemicals, significant cyclic thermomechanical stresses, and intense fluxes of high-energy neutrons and electromagnetic radiation. These structural materials typically feature highly complex and unique microstructures tailored for high-performance properties.

For example, the nanostructured ferritic alloys (NFAs), an emerging class of fusion structural material, exhibit remarkable radiation damage resistance and high-temperature tensile, creep and fatigue strengths [1,2]. NFAs derive from oxide dispersion strengthened (ODS)

Steels [3-10]. The outstanding performance characteristics of NFAs are attributed to the presence of an ultrahigh density of Y-Ti-O rich nanofeatures that are produced through carefully engineered and sophisticated mechanical alloying (MA) routes. NFAs and ODS alloys must be welded for construction of fusion reactors and other large-scale industry systems. However, these high-performance steels are very difficult, if not impossible, to weld with the conventional welding processes such as arc welding, laser welding and electron beam welding. The bulk melting in these fusion-welding processes inevitably destroys the fine particle distribution by causing the particles rejected and aggregated at the solidification front in weld pool. The poor fusion weldability has been the major technical bottleneck limiting the application of the entire ODS alloy family.

Reduced-activation ferritic/martensitic (RAFM) steels are considered as the reference first-wall and blanket structural material for both ITER test blanket modules and future fusion power systems in essentially all of the worldwide fusion materials research programs [11,12]. While considered to have relatively good weldability, RAFM steels can suffer from welding induced property degradations. Softening of the heat-affected zone (HAZ) is a major factor for performance degradation [13].

The plasma chamber of a fusion reactor will comprise different subsystems and modules that utilize different materials to meet the challenging performance requirements [11]. Dissimilar material joining – joining vastly different materials such as ODS/NFAs to RAFM steels – is central to successful development of fusion power systems but it also poses an even greater technological challenge in materials joining than joining ODS alloys or RAFM steels alone.

In this project, friction stir welding (FSW) technology, a solid-state joining process, was utilized to join ODS/NFAs, RAFM steels, and, in particular, dissimilar metal joining between ODS/NFAs and RAFM. Initial trials were made to develop the process space to consistently produce defect-free welds of ODS alloy, and develop the knowledge base and practical approaches to tailor and optimize the microstructure features in different zones of the welds to match the properties of the base metal through process innovation.

Experimental Procedure

FSW trails were made on the ODS alloy MA965, RAFM steels EUROFER97 and F82H. In addition, FSW was used to join MA956 to EUROFER97 (dissimilar weld). The FSW experimental matrix and basic welding conditions are summarized in Table 1. The thickness of MA956, EUROFER97 and F82H sheets are 1mm, 25mm and 8mm, respectively. Polycrystalline boron nitride was chosen as the welding tool material, due to its excellent hardness and thermal stability.

Table 1. Parameters used for FSW trials on different advanced steels.

Case No.	Material	Rotation Speed (rmp)	Travel Rate (ipm)	Tool Tilt Angle (°)	Plunge Depth (inch)	Note
1	EUROFER97	400	2	0.5	0.22	Tool A
2	MA956 to EUROFER97	400	2	0.5	0.22	Tool A pin was worn out.
3	F82H	400	2	0.5	0.208	Tool B
4	F82H	400	2.5	0.5	0.208	Tool B shoulder fractured.

Microstructures within the stir zone (SZ), thermo-mechanically affected zone (TMAZ), and HAZ were examined under optical microscope. Hardness mapping was also performed on the cross section of the welds using LM100AT micro-hardness tester, in order to reveal the effect of FSW on the mechanical property of ODS alloys and RAFM steels. Sample surface was grinded, polished, and etched with a mixture of 30ml HCl and 10ml HNO_3 for Cases 1 and 2, and Nital for Cases 3 and 4, to study the microstructure and to exam the welding defects.

Small-angle neutron scattering (SANS) measurements were conducted at CG-2 beamline of the High Flux Isotope Reactor (HFIR) at ORNL, in order to examine the influence of FSW on the dispersion of nano-scale particles in MA956 weld (made in this reporting period), as well as 14WT and 14YWT (made previously). Two specimens with a thickness of 0.4mm and an area of 5x5mm^2 were sliced out from the top and middle region of stir zone (SZ), respectively, for each friction stir welds. The neutron beam wavelength was 4.72Å, and sample to detector distances were 6 and 0.3 m. Magnetic field was applied along horizontal direction to differentiate the scattering amplitudes contributed by non-magnetic oxides from these contributed by the magnetic ferrous alloy matrix.

Results

Based on the optical microstructure examination, defect-free similar and dissimilar welds were successfully made in all the four cases. The microstructures in the SZ, TMAZ, and HAZ were significantly different from these in the base metal (BM). For instance, Figure 1 illustrates the optical micrographs of the dissimilar weld between MA956 and EUROFER97 (Case 2 in Table 1). The boundary of the SZ is highlighted by the blue dotted line. It is worth noticing that on the retreating side of the friction stir weld, a significant amount of the MA956, which is on the top of the EUROFER97, is stirred down to the bottom of stir zone, and embedded inside the EUROFER97 by the downward stirring motion of the threaded tool pin. It is noted that the original grains in the base metal of MA965 were very large, over several mm in the plane of the thin sheet. As shown in Figure 1 (a), (b) and (d), a few coarsened grains with a size larger than half millimeter are generated in the lower part of heat affected zone (HAZ) of MA956 on both the advancing and retreating sides. In comparison, Figure 1 (e) indicates that on the retreating side, there are no coarsened grains in the upper HAZ of MA956. After FSW, in the SZ, the grain size of MA956 is around 10μm, as shown in Figure 2 (c). As for EUROFER97, grain coarsening is observed in the SZ, by comparing its micrograph in Figure 2 (b) to that of the EUROFER97 base material (BM) in Figure 2 (d). In the SZ of F82H welds, which is now shown here, much refined grains were observed.

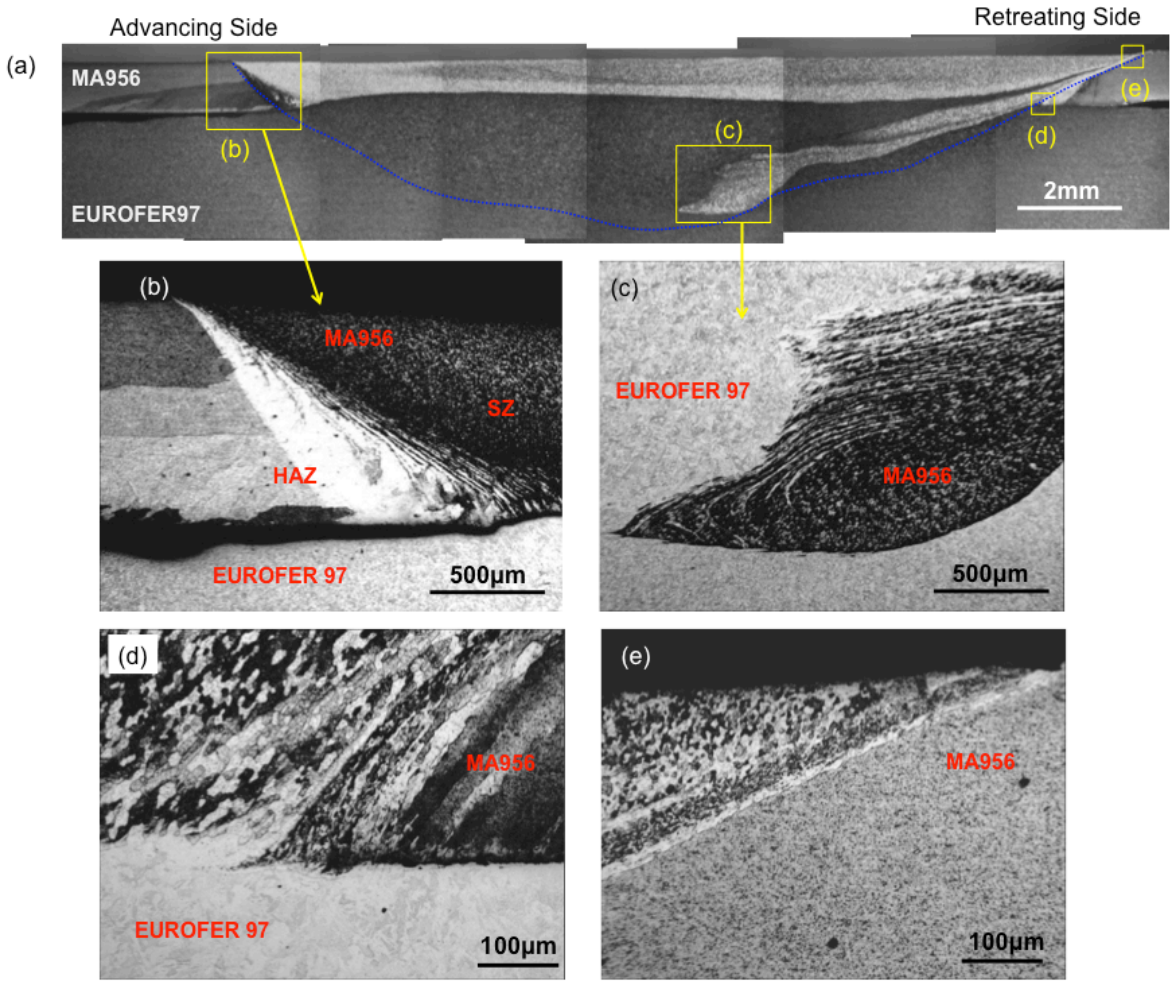

Figure 1. Optical micrographs of the dissimilar friction stir weld cross-section of MA956 to EUROFER97.

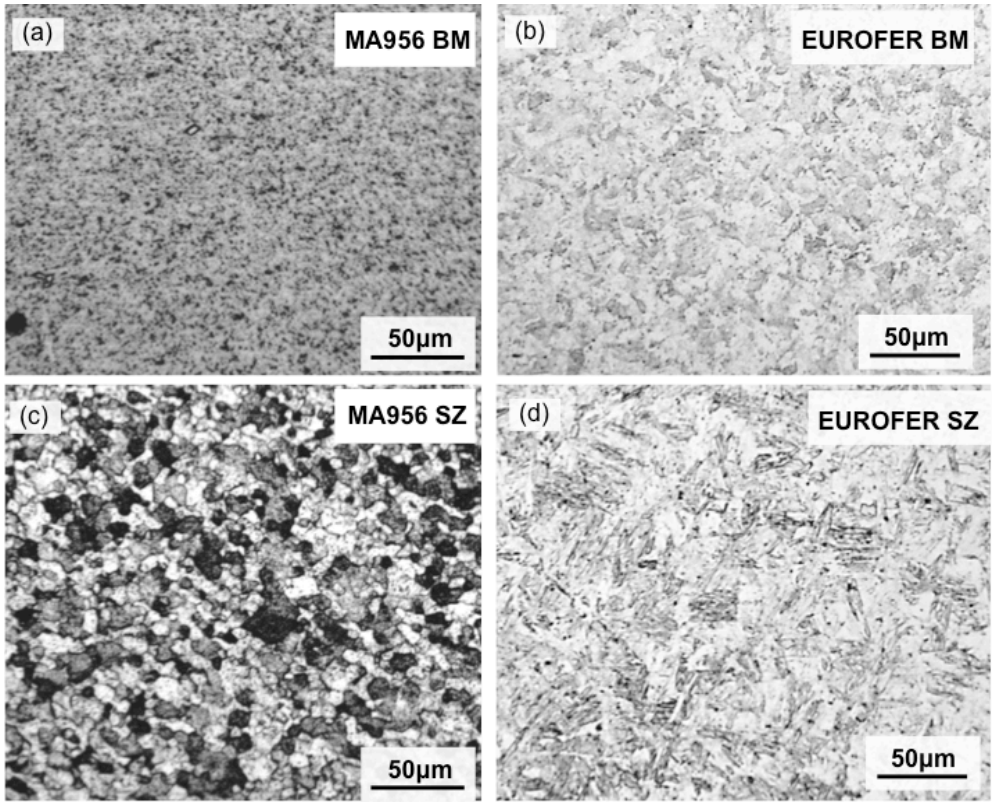

Figure 2. Optical micrographs of the base materials and stir zones of MA956 (a) and (c), and EUROFER97 (b) and (d), respectively, within the dissimilar friction stir weld of MA956 to EUROFER97.

Figures 3-6 show the micrographs of the welds cross sections of the four cases and their hardness distributions. Figure 7 summarizes the hardness profiles are plotted along the horizontal dotted lines marked in Figures 3-6 (b) within the upper part of the stir zone (SZ). Note that in Figure 7, x axis is the relative distance away from the center of SZ, as marked by the vertical dash dot lines in Figures 3-6 (b). As illustrated in Figures 3 (b), 4 (b) and 7(a), EUROFER97 base metal (BM) has an averaged hardness of ~220HV. FSW leads to a near twofold increase in the hardness within the SZ of EUROFER97. The highest hardness is observed on the retreating side of SZ. The boundary of thermo-mechanically affected zone (TMAZ) can be clearly identified in Figure 3(b), where the hardness in average is lower than that in SZ but higher than BM. A relatively large heat-affected zone (HAZ) with hardness lower than that of BM can be found outside the TMAZ, indicating softening in hardness and strength in the HAZ under the FSW conditions used in the welding trials. Figure 4(b) illustrates the hardness mapping on a dissimilar weld of MA956 and EUROFER97. MA956 BM has an averaged hardness ~268HV. After FSW, hardness of MA956, both on the top and in the middle of SZ, is decreased to as low as 190HV, as shown in Figures 4 (b) and 7 (a). Similar hardness distributions were observed within EUROFER97 welds in Cases 1 and 2. Figure 5 (b) shows that the F82H BM has an averaged hardness of ~320HV, and significant decrease in hardness was observed in HAZ. Note that for Case 4, the weld was made close to the edge of the F82H plate on the advancing side (AS). The relatively low thermal conductivity between steel and air leads to a more severe property degradation on the AS, as shown in Figure 6 (b).

By comparing Figure 6 (b) to Figure 5 (b), it can be concluded that faster travel rate, i.e., less heat input, during FSW results in higher hardness within SZ. Further characterization of the microstructure will be made to understand the hardness variation in different zones. FSW parameters will be modified to minimize the property degradation within HAZ.

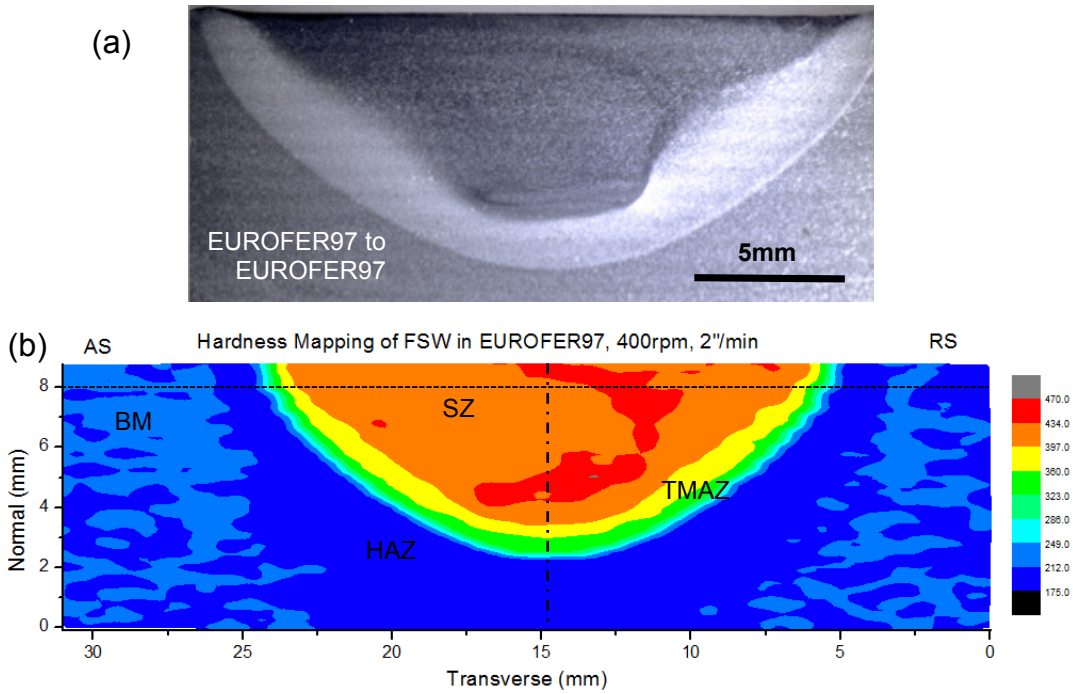

Figure 3. Friction stir welding of EUROFER97 (Case No. 1): (a) optical micrograph and (b) hardness mapping of the weld cross-section. AS and RS denote advancing and retreating sides. BM, SZ, TMAZ, HAZ represent base metal, stir zone, thermo-mechanically affected zone, and heat-affected zone.

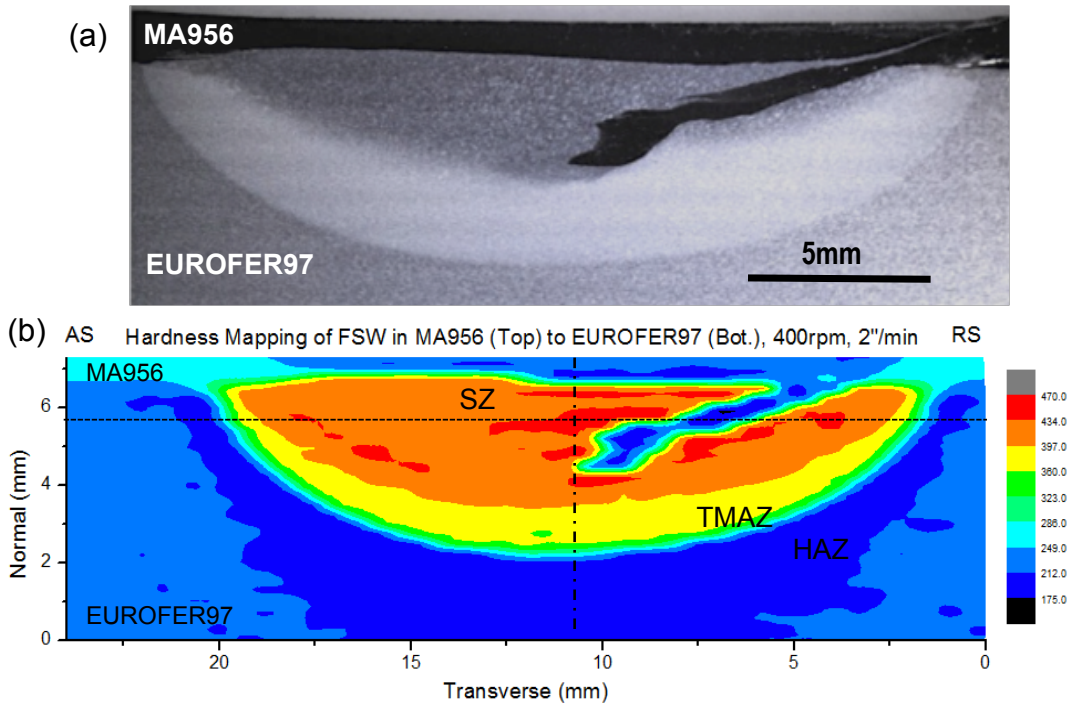

Figure 4. Friction stir welding of MA956 to EUROFER97 (Case No. 2): (a) optical micrograph and (b) hardness mapping of the weld cross-section.

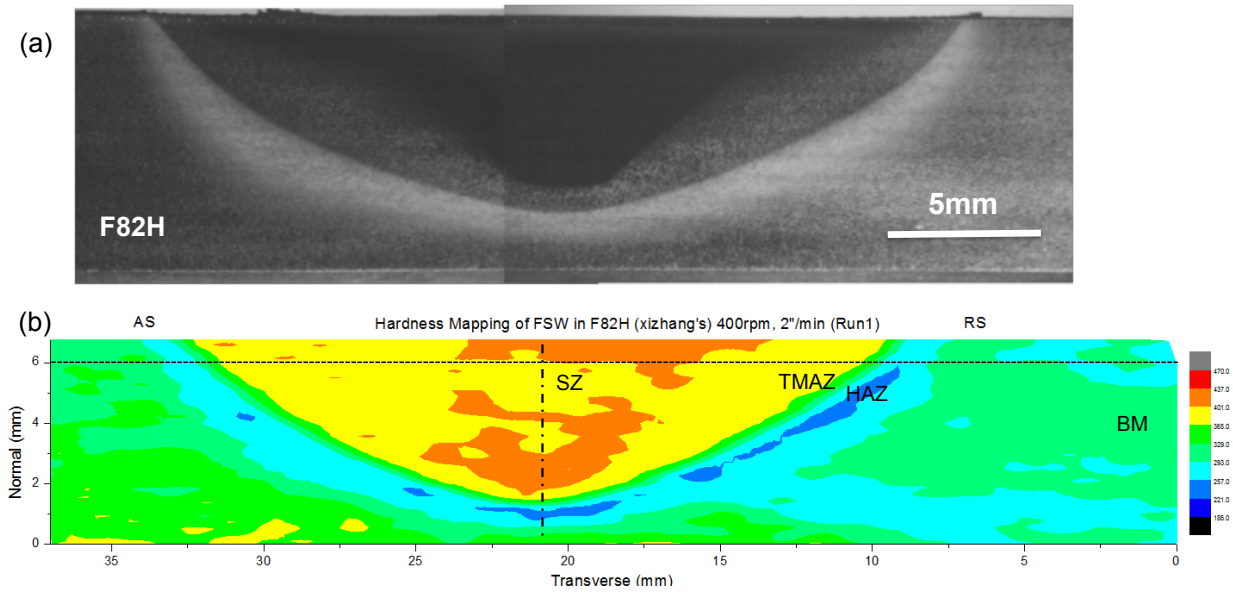

Figure 5. Friction stir welding of F82H (Case No. 3): (a) optical micrograph and (b) hardness mapping of the weld cross-section.

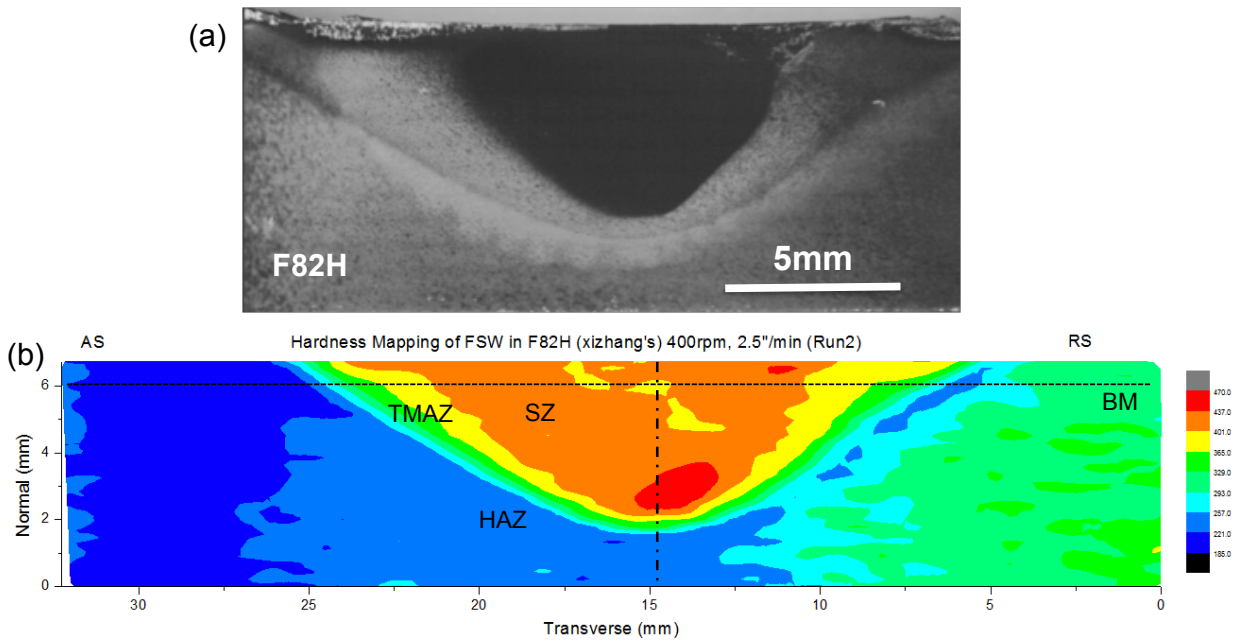

Figure 6. Friction stir welding of F82H (Case No. 4): (a) optical micrograph and (b) hardness mapping of the weld cross-section.

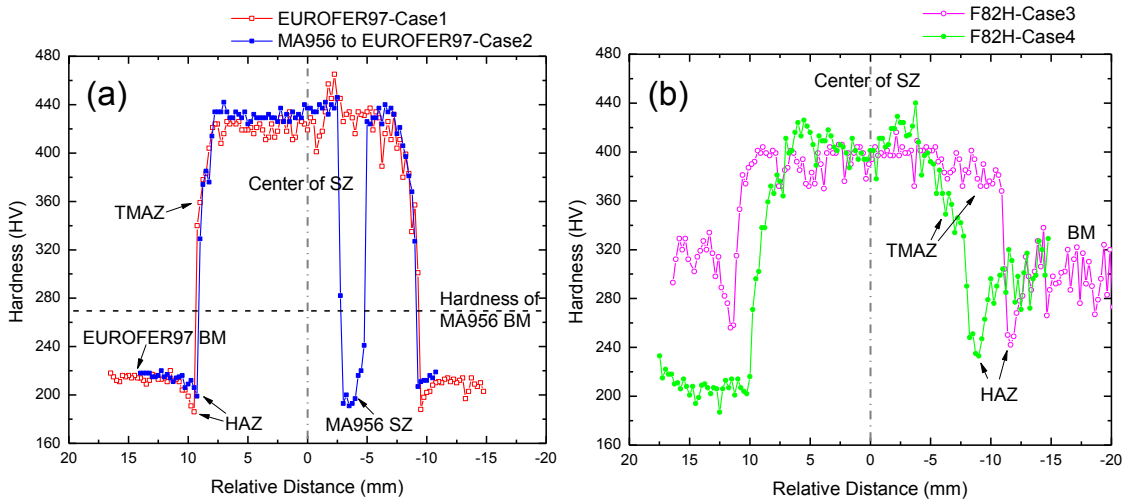

Figure 7. Hardness profile along the horizontal dotted lines marked in Figures 1-4 (b) within the upper part of SZ in the four cases.

Based on the hardness mapping result, it was observed that the selected FSW parameters led to reduction of hardness within the SZ of MA956. In order to reveal the effect of FSW on the dispersion of nano-particles, SANS measurements were performed in the BM and SZ of ODS alloys. Figure 8 (a)-(c) summarizes the obtained SANS images from the BM, top layer and 2nd layer of friction stir welds of 14WT. Data analysis is made on the SANS images, and the calculated probability of nano particles size are shown in Figure 8 (d)-(f). It indicates that in the

BM of 14WT, the nano particles are mostly about 3nm. Within the top layer of friction stir welds, the nano particles aggregate, and the mean size increases to near 5nm. In the second layer of friction stir welds, the nano particles are less influenced.

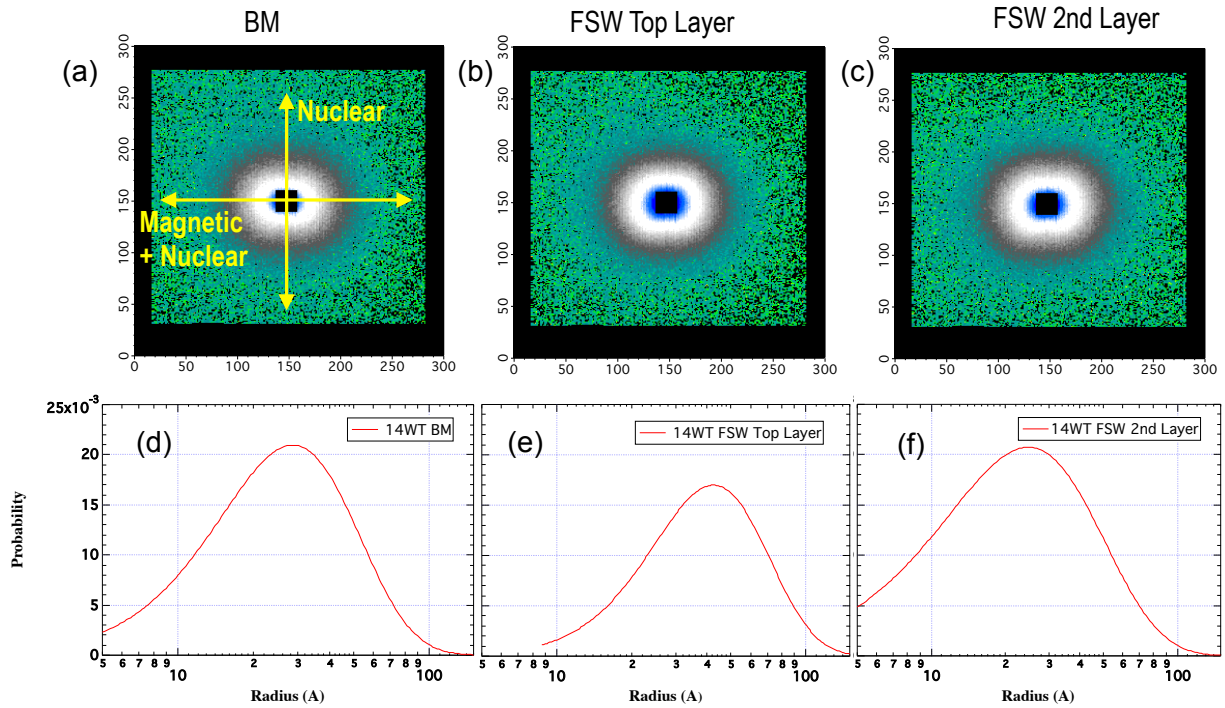

Figure 8. Small angle neutron scattering images (a)-(c) and the analyzed probability of nano particle size (d)-(f) in the BM, top layer and 2nd layer of friction stir welds in 14WT.

FUTURE WORK

Phases present in the SZ, TMAZ, HAZ and BM of EUROFER97, MA956 and F82H materials will be further analyzed through electron backscatter diffraction (EBSD) method. Also, more investigation will be made on the interface between the MA956 and EUROFER97 through scanning electron microscope (SEM) to reveal the bonding mechanisms in the dissimilar weld. Further analysis will be made in the SANS results of 14YWT and MA956 alloys.

REFERENCES

[1] G. R. Odette, M. J. Alinger, and B. D. Wirth, "Recent Development of Irradiation-Resistant Steels," *Annu. Rev. Mater. Res.* **38,** 417-503 (2008).
[2] G. R. Odette and D. T. Hoelzer, "Irradiation-Tolerant Nanostructured Ferritic Alloys: Transforming Helium from a Liability to an Asset," *JOM* **62** (9), 84-92 (2010).
[3] G. A. J. Hack, "Superalloys for the 80s," *Metallurgia.* **49** (6), 256-257 (1982).
[4] W. Sha and H. K. D. H. Bhadeshia, "Characterization of Mechanically Alloyed Oxide Dispersion-Strengthened Nickel-Base Superalloy MA760," *Metall. Mater. Trans. A* **25** (4), 705-714 (1982).

[5] M. J. Fleetwood, "Mechanical Alloying-the Development of Strong Alloys," *Mater. Sci. Tech.* **2** (12), 1176-1182 (1986).
[6] T. S. Chou and H. K. D. H. Bhadeshia, "Grain Control in Mechanically Alloyed Oxide Dispersion-Strengthened MA-957 Steel," *Mater. Sci. Tech.* **9** (10), 890-897 (1993).
[7] M. T. Shaw, "Incoloy Alloy MA956 for High Temperature Industrial Applications," *Metallurgia.* **54** (11), S32-S33 (1987).
[8] E. Grundy, C. J. Precious, and D. Finder, "Hot Forming of Mechanically Alloyed Gas Turbine Components," *Metal Powder Reports* **40** (10), 565-569 (1985).
[9] J. J. Fischer, "Properties of Mechanical Alloyed Super-Alloy Related to Industrial Heating Uses," *Ind. Heating* **40** (12), 25-26 (1988).
[10] R. K. Wilson and F. L. Perry, "Superior Heat Treatment Capabilities of MA Superalloys Developed by Thermo-Mechanical and Heat Treatment Processes," *Ind. Heating* **51** (5), 27-30 (1984).
[11] R. J. Kurtz, A. Alamo, E. Lucon, Q. Huang, and S. Jitsukawa, "Recent Progress Towards Development of Reduced Activation Ferritic/Martensitic Steels for Fusion Structural Applications," *J. Nucl. Mater.* **386-388**, 411-417 (2009).
[12] H. Serizawa, S. Nakamura, M. Tanaka, Y. Kawahito, H. Tanigawa, et al., "Effect of Mechanical Restraint on Weldability of Reduced Activation Ferritic/Martensitic Steel Thick Steels," *J. Nucl. Mater.* **417**, 55-88 (2011).
[13] N. Inoue, T. Muroga, A. Nishimura, and O. Motojima, "Correlation Between Microstructure and Hardness of a Low Activation Ferritic Steel (JLF-1) Weld Joint," *J. Nucl. Mater.* **258-263**, 1248-1252 (1998).